Clinical characteristics and pathological features of undetectable clinically significant prostate cancer on multiparametric magnetic resonance imaging: A single-center and retrospective study

Takahiro Yamamoto[1], Hiroaki Okada[1], Nozomu Matsunaga[1], Makoto Endo[2], Toyonori Tsuzuki[3], Keishi Kajikawa[4], Kojiro Suzuki[1]

Departments of [1]Radiology, [2]Radiological Technology, [3]Surgical Pathology and [4]Urology, Aichi Medical University, Nagakute, Aichi, Japan.

*Corresponding author:
Takahiro Yamamoto,
Department of Radiology, Aichi
Medical University, Nagakute,
Aichi, Japan.

yamamoto.takahiro.294@mail.
aichi-med-u.ac.jp

ABSTRACT

Objectives: The objectives of this study were to clarify the pathological features of clinically significant prostate cancer (csPC) that is undetectable on multiparametric magnetic resonance imaging (mpMRI).

Material and Methods: This single-center and retrospective study enrolled 33 men with prostate cancer (PC), encompassing 109 PC lesions, who underwent mpMRI before radical prostatectomy. Two radiologists independently assessed the mpMR images of all lesions and compared them with the pathological findings of PC. All PC lesions were marked on resected specimens using prostate imaging reporting and data system version 2.1 and classified into magnetic resonance imaging (MRI)-detectable and MRI-undetectable PC lesions. Each lesion was classified into csPC and clinically insignificant PC. Pathological characteristics were compared between MRI-detectable and MRI-undetectable csPC. Statistical analysis was performed to identify factors associated with MRI detectability. A logistic regression model was used to determine the factors associated with MRI-detectable and MRI-undetectable csPC.

Results: Among 109 PC lesions, MRI-detectable and MRI-undetectable PCs accounted for 31% (34/109) and 69% (75/109) of lesions, respectively. All MRI-detectable PCs were csPC. MRI-undetectable PCs included 30 cases of csPC (40%). The detectability of csPC on mpMRI was 53% (34/64). The MRI-undetectable csPC group had a shorter major diameter (10.6 ± 6.6 mm vs. 19.0 ± 6.9 mm, $P < 0.001$), shorter minor diameter (5.7 ± 2.9 mm vs. 10.7 ± 3.4 mm, $P < 0.001$), and lower percentage of lesions with Gleason pattern 5 (17% vs. 71%, $P < 0.001$). Shorter minor diameter (odds ratio [OR], 2.62; $P = 0.04$) and lower percentage of Gleason pattern 5 (OR, 24; $P = 0.01$) were independent predictors of MRI-undetectable csPC.

Conclusion: The pathological features of MRI-undetectable csPC included shorter minor diameter and lower percentage of Gleason pattern 5. csPC with shorter minor diameter may not be detected on mpMRI. Some MRI-undetectable csPC lesions exhibited sufficient size and Gleason pattern 5, emphasizing the need for further understanding of pathological factors contributing to MRI detectability.

Keywords: Gleason pattern, Magnetic resonance imaging, Prostate cancer, Pathology

INTRODUCTION

Prostate cancer (PC) can be classified as clinically significant PC (csPC) and clinically insignificant PC (ciPC). Curative therapies, such as radical prostatectomy, are indicated for csPC, whereas

active surveillance using serum prostate-specific antigen (PSA) is indicated for ciPC.[1,2] A new grading system for PC, which can predict cancer-specific mortality more accurately than the traditional Gleason scoring system, was approved by the International Society of Urological Pathology and the World Health Organization in 2014.[3] csPC has been defined as a tumor with a Gleason Score (GS) of ≥7 and diameter of ≥5 mm or a tumor with a GS of 3 + 3 and size ≥0.5 mL (tumor diameter ≥8 mm).[1] Multiparametric magnetic resonance imaging (mpMRI) with T2-weighted imaging (T2WI), diffusion-weighted imaging (DWI), and dynamic contrast-enhanced (DCE) magnetic resonance imaging (MRI) has been increasingly utilized for the detection and risk stratification of csPC in recent years.[4,5] The prostate imaging reporting and data system (PI-RADS) version 2.1 (v2.1) was released in 2019 by the American College of Radiology, European Society of Urogenital Radiology, and the AdMeTech Foundation to standardize image acquisition techniques, interpretation, and reporting of mpMRI.[6] Targeted biopsy of suspicious lesions visualized on mpMRI has been shown to improve the detection rate of csPC, and mpMRI may be used as a triage to avoid unnecessary systematic transrectal ultrasonography-guided biopsy.[7-11] However, 10–20% of missed lesions in patients with negative mpMRI have csPC of Grade ≥2.[9,12-14]

Large tumor volume, advanced stage, and high GS have been associated with intraductal carcinoma of the prostate (IDC-P).[15] IDC-P, an independent risk factor for progression-free and cancer-specific survival,[16] is considered to occur through the retrograde spreading of invasive carcinoma cells into benign glandular structures.[15,17] The cribriform subtype is a factor indicating poor prognosis. The 2014 International Society of Urological Pathology grading committee recommends that all cribriform subtype lesions should be staged as Gleason pattern 4.[3] IDC-P and the cribriform subtype are morphologically similar, suggesting that they may be identical or have similar pathologies.[17] Some studies have reported that ICD-P and the cribriform subtype affect the MRI detectability of PC, whereas others have not reported such findings; thus, whether these factors affect that the MRI detectability of PC remains unclear.[18-23] Therefore, in this study, we aimed to compare the pathology of MRI-detectable PC lesions with that of MRI-undetectable PC lesions to clarify the pathological features of csPC lesions that are undetectable on mpMRI.

MATERIAL AND METHODS

Patient selection

In total, 85 consecutive patients who had undergone radical prostatectomy at our hospital between January 2018 and December 2018 were retrospectively reviewed. Patients who met the following criteria were excluded: (1) prostate MRI examination performed at other hospitals; (2) prostate MRI examination performed more than 7 months prior at our hospital; (3) no DCE and poor images; and (4) biopsy performed before MRI. Figure 1 presents the patient selection flowchart. A total of 109 lesions were detected in 33 patients. The mean age of the patients was 70.7 ± 5.62 years, and the mean PSA level was 8 ± 4.13 ng/mL. Table 1 summarizes the clinical features of the study population and the pathological characteristics of PC lesions. This single-center and retrospective study was approved by the Local Institutional Review Board, and the required informed consent was obtained. This study was conducted in accordance with the tenets of the Declaration of Helsinki.

Histopathologic examination

Standard step sections of the specimens acquired through radical prostatectomy were obtained at 4–6-mm intervals, and the sections were stained with hematoxylin-eosin subsequently. Two pathologists recorded the tumor location, major and minor diameters of the tumor, GS of all tumor foci, and presence of IDC-P and cribriform subtype. The pathological map of PC, defined as a macroscopic photograph of the specimen on which all tumor lesions were marked, was created subsequently [Figure 2]. The results were evaluated by a uropathologist with more than 20 years of experience. GS was assigned according to the 2014 International Society of Urological Pathology Modified Gleason Grading System.[3]

MRI technique

A 3T scanner (MAGNETOM Skyra, Siemens Healthcare, Erlangen, Germany) or 1.5T scanner (MAGNETOM Aera or MAGNETOM Avant^Fit, Siemens Healthcare) with a combination of an 18-channel phased-array body coil and 32-channel spine
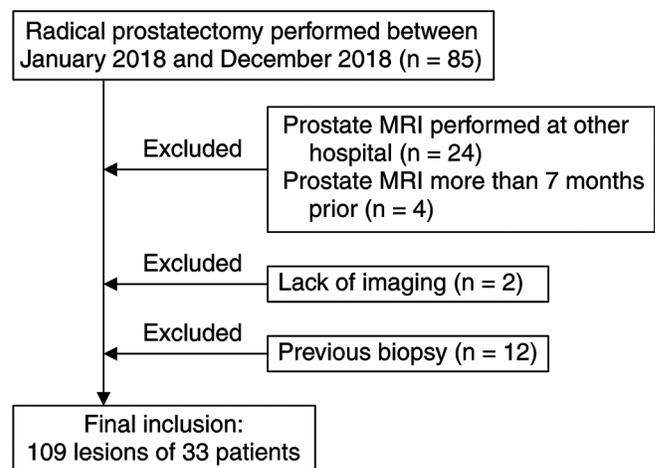
Figure 1: Patient selection flowchart. (MRI: Magnetic resonance imaging).
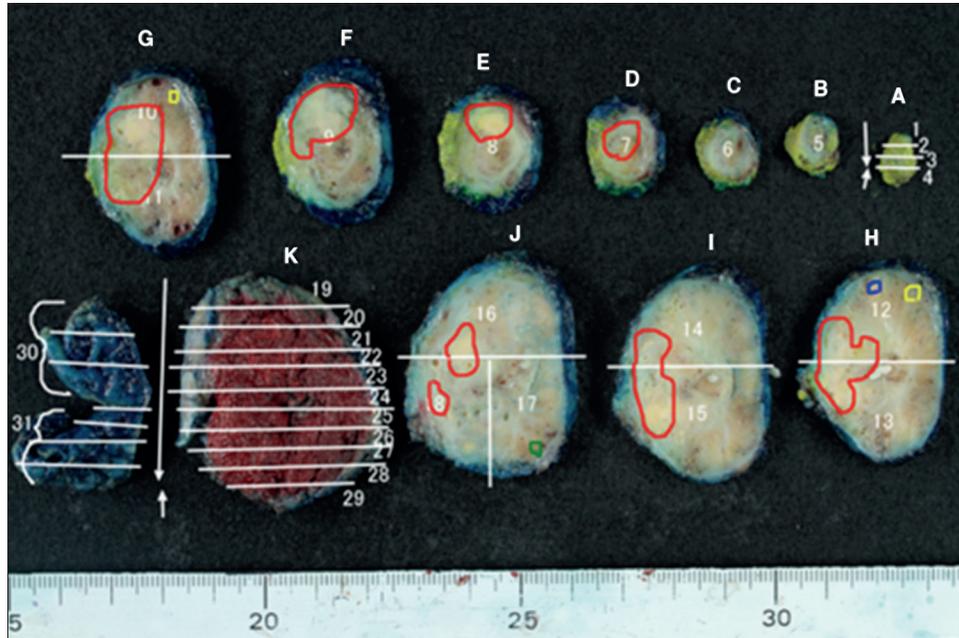
Figure 2: Pathological map of PC. (A-K and 1-31 are specimen identification codes. The white line is the excision line of the specimen. Four PC lesions detected on the pathological map of PC are illustrated in red, yellow, blue, and green.) (PC: Prostate cancer.)

coil were used to perform all MRI examinations. Overall, 23 and ten patients underwent MRI examinations with the 3T and 1.5T scanners, respectively. The images were acquired using the following pulse sequences: Axial turbo spin echo T2WI (3T: repetition time [TR]/echo time [TE], 4000/101 ms; slice thickness, 3 mm; no intersection gap; field of view [FOV], 200 × 200 mm, matrix, 320 × 304; acquisition pixel size, 0.66 × 0.63 mm; reconstruction pixel size, 0.31 × 0.31 mm; parallel imaging mode, Generalized Autocalibrating Partially Parallel Acquisitions [GRAPPA]; accel factor, 3. 1.5T: TR/TE, 3000/97 ms; slice thickness, 3 mm; no intersection gap; FOV, 220 × 220 mm; matrix, 320 × 256; acquisition pixel size, 0.86 × 0.69 mm; reconstruction pixel size, 0.34 × 0.34 mm; parallel imaging mode, GRAPPA; and accel factor, 2) and axial single-shot spin echo-planar DWI (3T: TR/TE, 6000/60 ms; slice thickness, 4 mm; no intersection gap; FOV, 220 × 176 mm; matrix, 100 × 76; acquisition pixel size, 2.32 × 2.20 mm; reconstruction pixel size, 1.1 × 1.1 mm; parallel imaging mode, GRAPPA; accel factor, 2; b values, 0 and 800 s/mm^2; and calculated high b value images [1500 s/mm^2]. 1.5T: TR/TE, 5500/70 ms; slice thickness 4 mm; no intersection gap; FOV, 240 × 216 mm; matrix, 100 × 90; acquisition pixel size, 2.40 × 2.40 mm; reconstruction pixel size, 1.20 × 1.20 mm; parallel imaging mode, GRAPPA, accel factor, 2; b values, 0 and 800 s/mm^2; and calculated high b value images [1500 s/mm^2]). The apparent diffusion coefficient (ADC) maps were created for b values of 0 and 800 s/mm^2 through mono-exponential fitting. The DCE images were acquired through axial 3D gradient echo T1WI. The DCE images were acquired every 10 s for 35 phases. The detailed parameters of image acquisition are listed in Table 2.

Image analysis

Two urologic radiologists with 7 years and 9 years of experience in prostate MRI, who were blinded to the clinical and histopathological findings, independently performed a retrospective evaluation of the mpMR images of the 109 lesions with reference to the pathological map of PC [Figure 2]. All mpMRI findings were assessed using PI-RADS v2.1.[6] The final decision was made by reaching a consensus in case of disagreements between the two radiologists. PC lesions with PI-RADS categories 3, 4, or 5 were classified as MRI-detectable PC lesions, whereas PC lesions with PI-RADS categories 1 or 2 were classified as MRI-undetectable PC lesions [Figure 3]. Figure 4 presents the study flowchart.

Statistical analysis

Fleiss kappa statistics was used to determine the interobserver agreement for the PI-RADS assessment category. The kappa values were defined as follows: Poor agreement, <0.20; fair agreement, 0.21–0.40; moderate agreement, 0.41–0.60; good agreement, 0.61–0.80; and excellent agreement, >0.80. The summary measurements are presented as means ± standard deviations. Student's *t*-test, Chi-squared test, or Fisher's exact test were used to compare the study groups. Two-tailed *P*-values were reported. A multivariate logistic regression model was used to identify the factors associated with MRI-detectable csPC or MRI-undetectable csPC lesions. All statistical analyses were performed using the Statistical Package for the Social Sciences for Windows (version 25;

IBM Corp., Armonk, NY, USA). The level of significance was set at $P < 0.05$.

Table 1: Clinicopathological characteristics of 109 prostate cancer lesions in 33 patients.

Number of patients	33
Age (years)[a]	70.7±5.62
Interval from MRI to prostatectomy (months)[a]	3±1.27
PSA level (ng/mL)[a]	8±4.13
MRI prostate volume (cm³)[a]	36.9±15.78
MRI PSA density (ng/mL/cm³)[a]	0.25±0.16
Number of prostate cancers	109
Size (mm)[a]	
Major diameter	10.2±8.54
Minor diameter	5.8±4.39
Lesion location[b] (%)	
PZ	85 (78)
TZ	17 (16)
PZ and TZ	7 (6)
Gleason score[b] (%)	
3+3	45 (41)
3+4	29 (26)
3+4 with 5	12 (11)
4+3	5 (5)
4+3 with 5	10 (9)
4+4	0
4+5	8 (7)
Pathological tumor stage[b] (%)	
T2	94 (86)
T3	15 (14)
IDC-P/Cribriform subtype[b] (%)	
IDC-P	7 (6)
Cribriform subtype	2 (2)
IDC-P and Cribriform subtype	11 (10)

[a]Data are presented as means±standard deviations, [b]Numbers in parentheses present the percentage values. IDC-P: Intraductal carcinoma of the prostate, PSA: Serum prostate-specific antigen, PZ: Peripheral zone; TZ: Transition zone, MRI: Magnetic resonance imaging. T2, T3: signify a pathological tumor stage and are in common use.

RESULTS

Among the 109 PC lesions, 31% (34/109) and 69% (75/109) were MRI-detectable and MRI-undetectable, respectively. The kappa value for interobserver agreement between the readers for the PI-RADS v2.1 assessment category was 0.79, indicating good agreement. All MRI-detectable PC lesions were csPC (34/34). csPC accounted for 40% (30/75) of MRI-undetectable PC lesions. The ciPC lesions could not be identified (45/45). Table 3 presents the pathological characteristics of MRI-detectable and MRI-undetectable csPC lesions. The major (10.6 ± 6.6 mm vs. 19 ± 6.9 mm, $P < 0.001$) and minor (5.7 ± 2.9 mm vs. 10.7 ± 3.4 mm, $P < 0.001$) diameters were shorter in the MRI-undetectable csPC lesions. Lesions with a minor diameter of ≤5 mm accounted for 53% (16/30) and 6% (2/34) of MRI-undetectable and MRI-detectable csPC lesions, respectively. In more detail, 50% (8/16) of MRI-undetectable csPC lesions with a minor diameter of ≤5 mm had a minor diameter of ≤4 mm. The percentage of MRI-undetectable csPC lesions with Gleason pattern 5 was low (17% vs. 71%, $P < 0.001$). The breakdown of lesions exhibiting Gleason pattern 5 similar to those with a GS of 9 (4 + 5) was as follows: 13% (4/30) of MRI-undetectable csPC lesions and 12% (4/34) of MRI-detectable csPC lesions. However, the occurrence of csPC lesions with tertiary pattern 5 among those with a GS of 7 (3 + 4 or 4 + 3) was 69% (20/29) and 5% (1/21) in the MRI-detectable and MRI-undetectable csPC groups. The pathological tumor stage of MRI-undetectable csPC lesions was significantly lower ($P < 0.001$). Notably, all T3 lesions were identifiable on MRI. Furthermore, the incidence of IDC-P and cribriform subtype was significantly lower (17% vs. 44%, $P = 0.018$) in MRI-undetectable csPC lesions. The cribriform subtype was detected in only one lesion in either group. The index lesion, defined as the most advanced PC lesion in the patient, was less frequent in patients with MRI-undetectable csPC lesions (17% vs. 71%, $P = 0.02$). No significant differences

Table 2: mpMRI pulse sequence parameters.

Imaging sequence	Pulse sequence	TR/TE (ms)	FOV (mm)	Matrix	Acquisition pixel size (mm)	Reconstruction pixel size (mm)	Slice thickness/ gap (mm)
3T							
T2WI axial	SE	4000/101	200×200	320×304	0.66×0.63	0.31×0.31	3.0/0
T2WI coronal	SE	4000/101	200×200	320×256	0.78×0.63	0.31×0.31	3.0/0
DWI	SE	6000/60	220×176	100×76	2.32×2.20	1.10×1.10	4.0/0
DCE	GRE	3.45/1.60	200×200	128×122	1.67×1.56	0.78×0.78	3.0
1.5T							
T2WI axial	SE	3000/97	220×220	320×256	0.86×0.69	0.34×0.34	3.0/0
T2WI coronal	SE	3000/95	220×220	320×224	0.98×0.69	0.34×0.34	3.0/0
DWI	SE	5500/70	240×216	100×90	2.40×2.40	1.20×1.20	4.0/0
DCE	GRE	4.00/1.79	220×192	128×101	1.97×1.72	0.86×0.86	3.0

DCE: Dynamic contrast enhanced, DWI: Diffusion-weighted imaging, FOV: Field of view, GRE: gradient echo, mpMRI: multiparametric magnetic resonance imaging, SE: Spin echo, T2WI: T2-weighted imaging, TE: Echo time; TR: Repetition time. T (tesla): represents a unit of magnetic force. It is a commonly used notation.
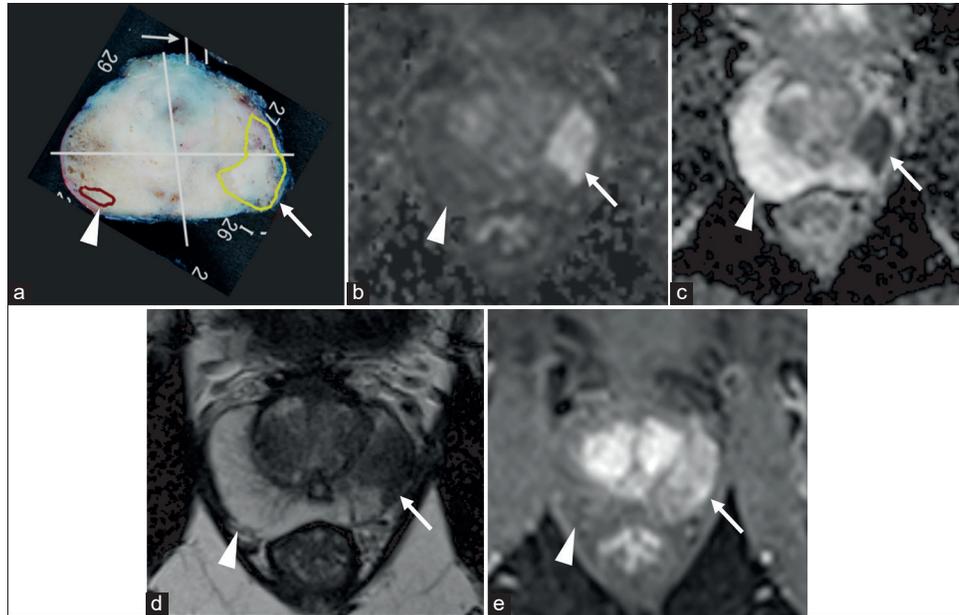
Figure 3: (a) Pathological map of PC, (b-e) mpMRI; (b) DWI, (c) ADC map, (d) T2WI, and (e) DCE. (a) Two lesions, one yellow and one brown, were detected on the pathological map of PC. The yellow lesion (white arrow) in the left peripheral zone showed hyperintensity on DWI, hypointensity on ADCmap, hypointensity on T2WI, and early enhancement on DCE. The yellow lesion (white arrow) was assessed as PI-RADS category 5 and classified as MRI-detectable PC. In contrast, the brown lesion (white arrow head) in the right peripheral zone showed no abnormal signal on mpMRI. The brown lesion (white arrow head) was assessed PI-RADS categories 1 and classified as MRI-undetectable PC. (ADC: Apparent diffusion coefficient, DCE: Dynamic contrast-enhanced, MRI: Magnetic resonance imaging, DWI: Diffusion-weighted imaging, mpMRI: multiparametric magnetic resonance imaging, PC: Prostate cancer, T2WI: T2-weighted imaging, PI-RADS: Prostate imaging reporting and data system.)
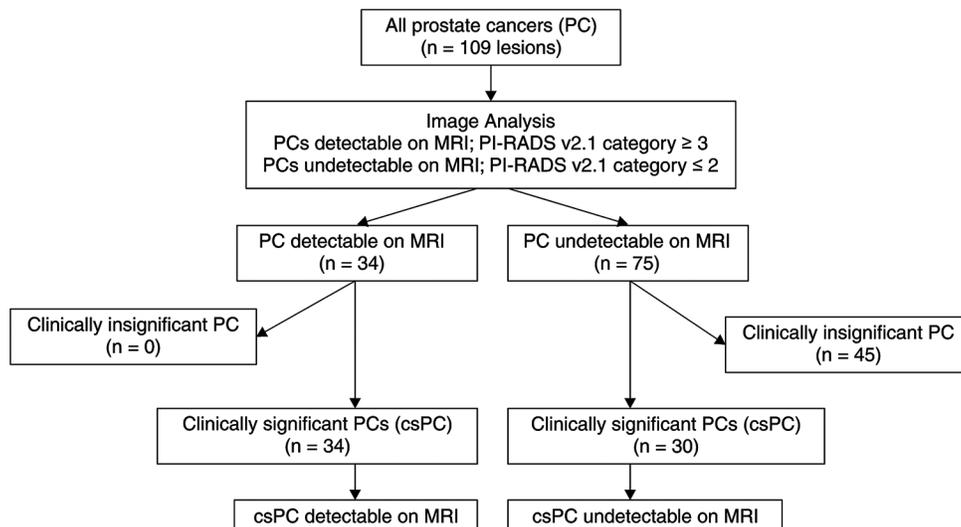
Figure 4: Flowchart of the study. (n: Number of lesions, csPC: Clinically significant prostate cancer, MRI: Magnetic resonance imaging, PI: prostate imaging, RADS: reporting and data system).

were observed among the remaining pathological features. Multivariate analysis revealed that the minor diameter (odds ratio [OR] 2.62; 95% confidence interval [CI]: 1.04, 6.62; *P* = 0.04) and Gleason pattern 5 (OR 24; 95% CI: 2.02, 292; *P* = 0.01) were factors associated with MRI-undetectable csPC lesions [Table 3]. No significant correlations were observed among the remaining pathological features. Four MRI-undetectable csPC lesions had a GS of 9 (4 + 5). The

Table 3: Pathological characteristics of detectable csPC and undetectable csPC on mpMRI.

	MRI-detectable csPC (*n*=34)	MRI undetectable csPC (*n*=30)	*P*-value from statistical tests	*P*-value from multivariable analysis	Odds ratio[c]
Size (mm)[a]			…	…	…
Major diameter	19.0±6.9	10.6±6.6	<0.001*	0.018	0.79 (0.56–1.11)
Minor diameter	10.7±3.4	5.7±2.9	<0.001*	0.04	2.62 (1.04–6.62)
Lesion location[b]			…	…	…
PZ	20 (59%)	23 (77%)	0.129**	…	…
TZ	8 (23%)	6 (20%)	0.733**	…	…
PZ and TZ	6 (18%)	1 (3%)	0.109***	…	…
Gleason score[b]			0.15**	0.24	0.39 (0.08–1.90)
6	1 (3%)	5 (17%)	…	…	…
7	29 (85%)	21 (70%)	…	…	…
8	0	0	…	…	…
9	4 (12%)	4 (13%)	…	…	…
Including pattern 5[b]	24 (71%)	5 (17%)	<0.001*	0.001	24 (2.02–292)
3+4 with 5	10 (29%)	1 (3%)	…	…	…
4+3 with 5	10 (29%)	0	…	…	…
4+5	4 (12%)	4 (13%)	…	…	…
Pathological tumor stage[b]			<0.001***	0.99	65×108 (0.00– ---)
T2	19 (56%)	30 (100%)	…	…	…
T3	15 (44%)	0	…	…	…
Index lesion[b]	24 (71%)	5 (17%)	0.02***	0.62	0.59 (0.07–4.71)
IDC-P/cribriform subtype	15 (44%)	5 (17%)	0.018**	0.98	1.03 (0.58–18.3)
IDC-P	5 (15%)	2 (7%)	…	…	…
Cribriform subtype	1 (3%)	1 (3%)	…	…	…
IDC-P and cribriform subtype	9 (26%)	2 (7%)	…	…	…

[a]Data are presented as means±standard deviations, [b]Numbers in parentheses present the percentage values, [c]Data in parentheses present the 95% confidence interval values. *Student's t-test. **χ^2 test, ***Fisher's exact test. csPC: Clinically significant prostate cancer, IDC-P: Intraductal carcinoma of the prostate, mpMRI: Multiparametric magnetic resonance imaging, PZ: Peripheral zone, TZ: Transition zone, with 5: Tertiary pattern 5. MRI: Magnetic resonance imaging, T2, T3: Signify a pathological tumor stage and are in common use.

mean size of the four MRI-undetectable csPC lesions with a GS of 9 (4 + 5) was 13.5 ± 6.2 mm × 4.7 ± 2.1 mm. The largest lesion of them was 20 mm × 8 mm. The other three of the lesions had a minor diameter of ≤5 mm. On the other hand, the mean size of the four MRI-detectable csPC lesions with a GS of 9 (4 + 5) was 24.5 ± 11.5 mm × 10.7 ± 3.8 mm. The smallest of those lesions was 13 mm × 5 mm.

DISCUSSION

Larger tumor size stands out as a primary indicator of successful detection on mpMRI.[24] The MRI-undetectable PC lesions were found to be smaller than the MRI-detectable PC lesions in previous studies, in consistency with our findings.[18,25] Kido *et al.* reported a mean tumor size of MRI-undetectable csPC lesions as 11.9 ± 4.0 mm.[25] The mean tumor size (major diameter) of MRI-undetectable csPC lesions was 10.6 ± 6.6 mm in the present study, which is a reasonable size for MRI-undetectable csPC lesions. Turkbey *et al.* reported that the detection of PC lesions <5 mm on mpMRI was poor.[26] The mean major diameter

of MRI-undetectable csPC lesions was 10.6 ± 6.6 mm in the present study, whereas the mean minor diameter was 5.7 ± 2.9 mm. To the best of our knowledge, no previous study has examined the minor diameter of csPC lesions. Multivariate analysis revealed a significant correlation between the minor diameter of the csPC lesions and decreased detectability on mpMRI (OR, 2.62; 95% CI, 1.04–6.62; *P* = 0.04). In our study, the proportion of the MRI-undetectable csPC lesions was 47% (30/64), which was higher than in previous reports. The reason for this was thought to be due to the large number of small lesions. About 53% (16/30) of the MRI-undetectable csPC lesions had a minor diameter of ≤5 mm, and another half (8/16) of those lesions had a minor diameter of ≤5 mm. This suggested that even if csPC lesions had a long enough major diameter, it would be difficult to detect on MRI if the minor diameter was <5 mm. Insufficient tumor volume may have contributed to the detectability of MRI.

Important pathological features of MRI-undetectable PC lesions typically involve less aggressive tumors, with a majority representing low-risk cancers characterized by a

GS of ≤6.[9,25,27-30] The percentage of PC lesions with tertiary pattern 5 in a GS of 7 was 69% (20/29) and 5% (1/21) in the MRI-detectable and MRI-undetectable csPC groups, respectively. The proportion of lesions with Gleason pattern 5 was significantly lower in the MRI-undetectable csPC group (17% vs. 71%, $P < 0.001$), suggesting a comparatively lower risk profile for MRI-undetectable csPC lesions relative to their MRI-detectable csPC lesions.

Truong *et al.* first reported that IDC-P and the cribriform subtype hindered the detectability of PC on mpMRI.[18] However, some studies have reported that IDC-P and the cribriform subtype reduced the detection rate of tumors, whereas others have reported that they did not affect the detectability of tumors, with recent studies predominantly reporting that IDC-P does not affect the detectability of tumors.[19-23,31] In our study, the presence of IDC-P and the cribriform subtype did not affect the detectability of csPC lesions on mpMRI. Notably, these histological features were more frequently observed in MRI-detectable csPC lesions compared to their MRI-undetectable counterparts (44% vs. 17%, $P = 0.018$), aligning with expectations given their association with larger and more advanced lesions.[15] However, only one lesion each with the cribriform subtype was present in the MRI-detectable and MRI-undetectable csPC groups; thus, the effect of the cribriform subtype must be examined further.

In our study, four undetectable csPC lesions had a GS of 9 (4 + 5). The mean size of the four tumors was 13.5 ± 6.2 mm × 4.7 ± 2.1 mm, and the minor diameter was ≤5 mm in three tumors. This finding suggests that csPC lesions with a GS of 9 and a short minor diameter are undetectable on mpMRI. However, one tumor was 20 mm × 8 mm in size, which is sufficiently large to be detected on MRI [Figure 5]. Although not considered in the present study, this tumor might be a lesion with a low density of cancer cells.[21,31] A subset of MRI-undetectable csPC lesions exhibited sufficient size and harbored Gleason pattern 5. Unfortunately, there is currently no established MRI technique specifically tailored for detecting these lesions. It is important to consider pathologic findings other than the pathological features discussed here to fully elucidate the causes of failure to identify csPC on mpMRI.

This study has some limitations. First, this was a single-center and retrospective study with a relatively small sample size. Second, there is a possibility of overestimation of MRI-detectable PC lesions as the pathological map of PC was used for lesion detection on mpMRI. Furthermore, lesion morphology concordance, that is, whether any part of the lesion depicted on the pathological map could be discerned by mpMRI, was not assessed, leading to classification of lesions as MRI-detectable PC lesions. Finally, the areas of csPC identified on MRI were not cross-referenced with pathological features, thus the inclusion of Gleason pattern 5 in the identified areas.
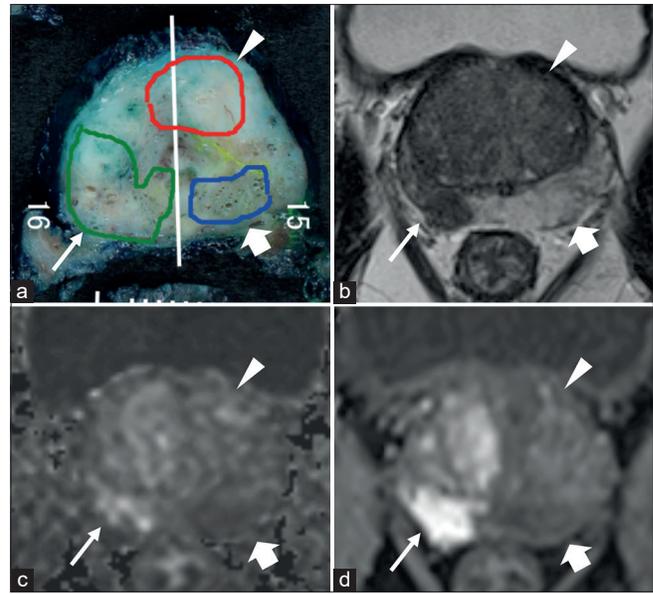
Figure 5: (a) Pathological map of PC, (b-d) mpMRI; (b) T2WI, (c) DWI, and (d) DCE. (a) Three lesions, one green, one red, and one blue, were detected on the pathological map of PC. (a) The white line is the excision line of the specimen. The Gleason score for all three lesions were 9 (4+5). The green lesion (thin white arrow) was MRI-detectable csPC, approximately 43 mm × 10 mm in size. The red lesion (white arrow head) and blue lesion (thick white arrow) lesions were MRI undetectable csPC, approximately 20 mm × 8 mm and 19 mm × 5 mm in size, respectively. (DCE: Dynamic contrast-enhanced, MRI: Magnetic resonance imaging, DWI: Diffusion-weighted imaging, mpMRI: Multiparametric magnetic resonance imaging, PC: Prostate cancer, T2WI: T2-weighted imaging, csPC: Clinically significant prostate cancer).

CONCLUSION

This study demonstrated that the pathological features of MRI-undetectable csPC include shorter minor diameter and lower proportion of lesions with Gleason pattern 5. However, a small number of MRI-undetectable csPC lesions were of sufficient size and had Gleason pattern 5. Thus, it is crucial to consider pathologic findings other than the pathological features discussed here to fully elucidate the causes of failure to identify csPC lesions on mpMRI.

Ethical approval

The research/study approved by the Institutional Review Board at Aichi Medical University Hospital, number 2021–005, dated April 15, 2021.

Declaration of patient consent

The authors certify that they have obtained all appropriate patient consent.

Financial support and sponsorship

Nil.

Conflicts of interest

There are no conflicts of interest.

Use of artificial intelligence (AI)-assisted technology for manuscript preparation

The authors confirm that there was no use of artificial intelligence (AI)-assisted technology for assisting in the writing or editing of the manuscript and no images were manipulated using AI.

REFERENCES

1. Weinreb JC, Barentsz JO, Choyke PL, Cornud F, Haider MA, Macura KJ, *et al.* PI-RADS prostate imaging-reporting and data system: 2015, version 2. Eur Urol 2016;69:16-40.
2. Mottet N, Bellmunt J, Bolla M, Briers E, Cumberbatch MG, De Santis M, *et al.* EAU-ESTRO-SIOG guidelines on prostate cancer. Part 1: Screening, diagnosis, and local treatment with curative intent. Eur Urol 2016;71:618-29.
3. Epstein JI, Egevad L, Amin MB, Delahunt B, Sigley JR, Humphrey PA, *et al.* The 2014 International Society of Urological Pathology (ISUP) consensus conference on Gleason grading of prostatic carcinoma: Definition of grading patterns and proposal for a new grading system. Am J Surg Pathol 2016;40:244-52.
4. Renard-Penna R, Rouviere O, Puech P, Borgono C, Abbas L, Roy C, *et al.* Current practice and access to prostate MR imaging in France. Diagn Interv Imaging 2016;97:1125-9.
5. Oberlin DT, Casalino DD, Miller FH, Meeks JJ. Dramatic increase in the utilization of multiparametric magnetic resonance imaging for detection and management of prostate cancer. Abdom Radiol 2017;42:1255-8.
6. Turkbey B, Rosenkrantz AB, Haider MA, Tempany CM, Choyke PL, Cornud F, *et al.* Prostate imaging reporting and data system version 2.1: 2019 update of prostate imaging reporting and data system version 2. Eur Urol 2019;76:340-51.
7. Siddiqui MM, Rais-Bahrami S, Turkbey B, George AK, Rothwax J, Shakir N, *et al.* Comparison of MRI/ultrasound fusion-guided biopsy with ultrasound-guided biopsy for the diagnosis of prostate cancer. JAMA 2015;313:390-7.
8. Wegelin O, van Melick HH, Hooft L, Bosch JL, Reitsma HB, Barentsz JO, *et al.* Comparing three different techniques for magnetic resonance imaging-targeted prostate biopsies: A systematic review of in-bore versus magnetic resonance imaging-transrectal ultrasound fusion versus cognitive registration. Is there a preferred technique? Eur Urol 2017;71:517-31.
9. Ahmed HU, El-Shater Bosaily A, Brown LC, Gabe R, Kaplan R, Parmar MK, *et al.* Diagnostic accuracy of multi-parametric MRI and TURS biopsy in prostate cancer (PROMIS): A paired validating confirmatory study. Lancet 2017;389:815-22.
10. Kasivisvanathan V, Rannikko AS, Borghi M, Panebianco V, Mynderse LA, Vaarala MH, *et al.* MRI-targeted or standard biopsy for prostate-cancer diagnosis. N Engl J Med 2018;378:1767-77.
11. Rouvière O, Puech P, Renard-Penna R, Claudon M, Roy C, Mege-Lechevallier F, *et al.* Use of prostate systematic and targeted biopsy on the basis of multiparametric MRI in biopsy-naive patients (MRI-FIRST): A prospective, multicentre, paired diagnostic study. Lancet Oncol 2019;20:100-9.
12. Padhani AR, Barentsz J, Villeirs G, Rosenkrantz AB, Margolis DJ, Turkbey B, *et al.* PI-RADS steering committee: The PI-RADS multiparametric MRI and MRI-detected biopsy pathway. Radiology 2019;292:464-74.
13. Park KJ, Kim MH, Kim JK, Cho KS. Characterization and PI-RADS version 2 assessment of prostate cancers missed by prebiopsy 3-T multiparametric MRI: Correlation with whole-mount thin-section histopathology. Clin Imaging 2019;55:174-80.
14. Mohammadian Bajgiran A, Afshari Mirak S, Shakeri S, Felker ER, Ponzini D, Ahuja P, *et al.* Characteristics of missed prostate cancer lesion on 3T multiparametric-MRI in 518 patients: Based on PI-RADSv2 and using whole-mount histopathology reference. Abdom Radiol (NY) 2019;44:1052-61.
15. Tsuzuki T. Intraductal carcinoma of the prostate: A comprehensive and updated review. Int J Urol 2015;22:140-5.
16. Kimura K, Tsuzuki T, Kato M, Saito AM, Sassa N, Ishida R, *et al.* Prognostic value of intraductal carcinoma of the prostate in radical prostectomy specimens. Prostate 2014;74:680-7.
17. Kweldam CF, Kümmerlin IP, Nieboer D, Verhoef EI, Steyerberg EW, van der Kwast TH, *et al.* Disease-specific survival of patients with invasive cribriform and intraductal prostate cancer at diagnostic biopsy. Mod Pathol 2016;29:630-6.
18. Truong M, Hollenberd G, Weinberg E, Messing EM, Miyamoto H, Frye TP. Impact of Gleason subtype on prostate cancer detection using multiparametric magnetic resonance imaging: Correlation with final histopathology. J Urol 2017;198:316-21.
19. Truong M, Feng C, Hollenberg G, Weinberg E, Messing EM, Miyamoto H, *et al.* A comprehensive analysis of cribriform morphology on magnetic resonance imaging/ultrasound fusion biopsy correlated with radical prostatectomy specimens. J Urol 2018;199:106-13.
20. Tonttila PP, Ahtikoski A, Kuisma M, Pääkkö E, Hirvikoski P, Vaarala MH. Multiparametric MRI prior to radical prostatectomy identifies intraductal and cribriform growth patterns in prostate cancer. BJU Int 2019;124:992-8.
21. Mikoshi A, Miyai K, Hamabe F, Edo H, Ito K, Matsukuma S, *et al.* MRI-detectability and histological factors of prostate cancer including intraductal carcinoma and cribriform pattern. Prostate 2022;82:452-63.
22. Currin S, Flood TA, Krishna S, Ansari A, McInnes MD, Schieda N. Intraductal carcinoma of the prostate (IDC-P) lowers apparent diffusion coefficient (ADC) values among intermediate risk prostate cancers. J Magn Reson Imaging 2019;50:279-87.
23. Arslan A, Alis D, Tuna MB, Sağlıcan Y, Kural AR, Karaarslan E. The visibility of prostate cancer concerning underlying histopathological variances: A single-center mutiparametric magnetic resonance imaging study. Eur J Radiol 2021;141:109791.
24. Martorana E, Pirola GM, Scialpi M, Micali S, Iseppi A,

Bonetti LR, *et al.* Lesion volume predicts prostate cancer risk and aggressiveness: Validation of its value alone and matched with prostate imaging reporting data system score. BJU Int 2017;120:92-103.

25. Kido A, Tamada T, Kanomata N, Yamamoto A, Miyaji Y, Nagai A, *et al.* Multidimensional analysis of clinicopathological characteristics of false-negative clinically significant prostate cancers on multiparametric MRI of the prostate in Japanese men. JJR 2019;37:154-64.

26. Turkbey B, Mani H, Shah V, Rastinehad AR, Bernardo M, Pohida T, *et al.* Multiparametric 3T prostate MR imaging to detect cancer: Histopathologic correlation using prostatectomy specimens processed in customized MRI-Based molds. J Urol 2011;186:1818-24.

27. Zelhof B, Pickles M, Liney G, Gibbs P, Rodrigues G, Kraus S, *et al.* Correlation of diffusion-weighted magnetic resonance data with cellularity in prostate cancer. BJU Int 2009;103:883-8.

28. Tamada T, Prabhu V, Li J, Babb JS, Aneja SS, Rosenkrantz AB. Prostate cancer: Diffusion-weighted MR imaging for detection and assessment of aggressiveness-comparison between conventional and kurtosis models. Radiology 2017;284:100-8.

29. Tamada T, Dani H, Taneja SS, Rosenkrantz AB. The role of whole-lesion apparent diffusion coefficient analysis for predicting outcomes of prostate cancer patient on active surveillance. Abdom Radiol (NY) 2017;42:2340-5.

30. Tamada T, Kanomata N, Sone T, Jo Y, Miyaji Y, Higashi H, *et al.* High b value (2,000 s/mm^2) diffusion-weighted magnetic resonance imaging in prostate cancer at 3Tesla: Comparison with 1,000 s/mm^2 for tumor conspicuity and discrimination of aggressiveness. PLoS One 2014;9:e96619.

31. Miyai K, Mikoshi A, Hamabe F, Nakanishi K, Ito K, Tsuda H, *et al.* Histological differences in cancer cells, stroma, and luminal spaces strongly correlate with *in vivo* MRI-detectability of prostate cancer. Mod Pathol 2019;32:1536-43.